Comparative Performance Study of Nanoantennas

Alexandra Pereira
Instituto Superior Técnico
{alexandra.c.pereira@tecnico.ulisboa.pt}

***Abstract*—To overcome the restriction of the power conversion efficiency of solar cells, several approaches have been proposed one of which being the integration of nanoantennas. Due to the formation of surface plasmon polaritons and the extraordinary optical transmission phenomenon, nanoantennas are capable of locally enhancing the electromagnetic field. Since the discovery of nanoantennas, some geometries have been developed to improve device operation and thus achieve higher power conversion. This work aims to analyze and compare two designs of slot nanoantennas coupled to an amorphous silicon layer and obtain the simulation results of the optical response to infer the effect nanoantennas can have on solar cells. To achieve this, two nanoantenna geometries were modelled using *COMSOL Multiphysics*® to simulate their behaviour in a standalone setting before being integrated with an amorphous silicon layer. Some geometric parameters were varied to infer their influence on the optical response of the nanoantennas. The simulation results demonstrate that the geometric parameters can influence the resonance of the nanoantennas and that coupling them onto the absorber layer can improve light capture and ultimately improve solar energy absorption in solar cells.**

***Index Terms*—Photovoltaic technology, Optical rectennas, Multi-junction solar cell, nanoantenna, Surface plasmons, Extraordinary optical transmission.**

I. Introduction

THE most basic form of photovoltaic technology is a single junction of crystalline silicon which, due to its properties, can only ever achieve a maximum of 29.42% of power conversion efficiency, as established by the Shockley-Queisser limit. To overcome this limitation, researchers have developed multi-junction solar cells with materials with complementing absorption ranges, and in recent years high-efficiency solar cells, reaching 39.2% under one sun and 47.1% under concentration, have been developed. [1]

Another approach to increase absorbed radiation is optical rectennas, composed of a rectifier in series with a nanoantenna.

The sunlight Electromagnetic (EM) spectrum ranges from 100 nm to 1 mm meaning the antenna must be scaled down to the nanoscale in order to harvest the desired wavelength. In the early stages of the development of these devices miniaturization proposed a problem, but with the years and the evolution of the nanotechnology it is no longer a concern.

In high frequency (GHz and THz) the penetration of the EM waves in the metals cause oscillation of conducting electrons which then form plasmon and induce resonance. This to say that the metals used for the antenna, in high-frequency operation, can no longer be under the perfect conductor approximation [2].

A plasmon is the quantization of plasma oscillation. It appears when electrons are excited by the incident photons. They oscillate back and forth creating an oscillation of the free electron gas. When a plasmon interacts with a nanoparticle inside the metal it gives rise to a localised oscillation resulting in a resonance effect with a localized field amplification in and near the nanoparticle [2], [3]. The shape of the antenna can optimize this phenomena and as such several designs have been developed to improve its operation.

A. Nanoantenna Designs

To make use of the field amplification phenomena caused by surface plasmons, nanoantennas are made with plasmonic materials, usually, metals selected to support resonance at the desired frequency. For optical frequencies, gold, silver and aluminium are mostly used. Research shows that field intensity is higher between two nanoparticles, and as such, several nanoantenna designs have been developed [4].

1) Aperture Nanoantennas: These nanoantennas focus the EM waves onto an aperture thus allowing light confinement and control of the radiation pattern [5]. This type of nanoantenna can be divided into three main sub-groups:

- **Single subwavelength aperture** - a metal chosen according to the desired wavelength operation is perforated in circular holes, slits, rectangles, or triangles [6]. The apertures focus radiation which enables light confinement thus improving the coupling efficiency of the antenna [5].
- **Single aperture surrounded by shallow surface corrugations** - corrugations are added to the surface area around the aperture. The corrugations extend the abilities of the previous aperture design by also allowing near to far-field conversion, a valuable addition to the light confinement capabilities of the aperture [6].
- **Subwavelength aperture arrays** - the apertures are distributed with periodic lattice which helps match the surface EM waves to the far-field radiation. This extends the coupling abilities of the aperture nanoantenna. Parameters like hole size and shape, metal type, and lattice constant are highly important to obtain the desired operation of the antenna[6].

II. Diffraction Theories

A. Huygens-Fresnel Principle

In the XVII century, Hyugen developed a theory stating that in a wave front, each point emits spherical secondary wavelets, with the same characteristics as the primary wave, which combine and create a new wave front in the direction of propagation. However, as light encountered a medium with edges, slits, or apertures, deviations from rectilinear

propagation, called diffraction effects, were verified which the theory failed to explain. In the XVIII century, Hyugen's theory was reformulated by Fresnel who theorized that near slits or apertures, the wave was not plane. The combination of both theories explained the rectilinear propagation of light and diffraction effects [7], [8], [9] creating the Huygen-Fresnel Principle which serves as baseline for diffraction theories.

B. Young's Experiment

In 1803 before Fresnel presented his work on interference theory, Thomas Young had already provided experimental results for the wave theory of light. In his experiment, denominated double slit experiment, or interference experiment, light is made to shine upon a metal plane with two slits and a target parallel to the plane. Based on Hyugen's Principle, the slits radiate spherical waves that interact with each other. Young theorized destructive interference if the waves were 180º out of phase (meeting crest-to-trough) where they would cancel out each other and leave a dark spot on the screen target. If on the contrary, the waves were in phase (meeting crest-to-crest) Young expected constructive interference and a bright spot on the screen target. Conducting the experiments, Young was able to prove his theories [10].

C. Fraunhofer Diffraction Equation

While Fresnel's diffraction theory applies to the near-field regime, Fraunhofer's diffraction theory is used to model the diffraction in the far-field region.

Fraunhofer's theory proposed the ability to characterize the irradiance on y' axis of a monochromatic wave passing through a slit of diameter a with normal incidence. The metal plane was considered a perfect conductor, and the wave was characterized by λ_0 as the incident wavelength and k the wavevector [11], [9].

He related the irradiance with the angle of diffraction θ and the main lobe ($\theta = 0$) with equation (1).

$$I(\theta) = I(0)\left(\frac{sin(\beta)}{\beta}\right)^2 \tag{1}$$

$$\beta = \frac{ka}{2}sin(\theta) \tag{2}$$

$$k = \frac{2\pi}{\lambda_0} \tag{3}$$

Additionally, the theory could be reformulated into equation (4) for an array of N splits, equally spaced by d [9].

$$I(\theta) = I_0\left(\frac{sin(\beta)}{\beta}\right)^2\left(\frac{sin(N\alpha)}{\alpha}\right)^2 \tag{4}$$

$$\alpha = \frac{kd}{2}sin(\theta) \tag{5}$$

The characterization of the irradiance $I(\theta)\langle E^2\rangle$ is an important achievement as it allows to compare theory to simulations results.

D. Kirchhoff Diffraction Theory

In 1887, Kirchhoff developed a theory based on Fresnel and Fraunhofer's theories capable of obtaining results for the Hyugens-Fresnel theory. The theory considered a scalar wave equation (eq.6) approximation on the x direction and an opaque plane perpendicular to it[11], [9].

$$\nabla^2\bar{\psi} + k_0^2\bar{\psi} = 0 \tag{6}$$

To find the solution, Kirchhoff used the Green theorem represented in eq.7 where S is the surface, assuming it extends to infinite.

$$\Psi(r) = \frac{1}{4\pi}\int\left[\frac{\partial\bar{\psi}}{\partial\mathbf{n}}\frac{e^{ik_0r}}{r} - \bar{\psi}\frac{\partial}{\partial\mathbf{n}}\frac{e^{ik_0r}}{r}\right]dS \tag{7}$$

Being ψ_0 the field intensity of the incident wave, Kirchhoff considered the following approximations: noitemsep

- For the right side of the surface: $\psi = 0$ and $\frac{\partial\bar{\psi}}{\partial n} = 0$
- In the slit region: $\psi = \psi_0$

The assumptions made above mean the screen is neglected, which simplifies the problem. However, it makes the field zero behind the screen except in the aperture which in turn results in a discontinuous Ψ and $\partial\Psi/\partial n$ on the boundary of the aperture. Additionally, the values of Ψ and $\partial\Psi/\partial n$ are based on assumptions and as such produce only approximate solutions for the diffraction problem [7]. Although the Kirchhoff theory produces good results for large slits (compared to the wavelength), it is no longer valid for subwavelength slits [11], [9].

E. Bethe-Bouwkamp Diffraction Theory

In 1944, with the intention of overcoming the limitations of Kirchhoff's theory, Bethe proposed a new theory for a circular aperture in a perfect conductive metal surface making 3 base assumptions [11]:

- Incident and reflected waves exist over the metal surface
- Metal conductivity is infinite and as such, electromagnetic waves do not penetrate the surface
- Electric field $\bar{\mathbf{E}}$ tangential to the surface and magnetic field $\bar{\mathbf{H}}$ perpendicular to the surface

With it's calculations, Bethe proved that it was possible to calculate the electromagnetic field in and around the aperture. However, later analysing the theory, Bouwkamp found discontinuities in the boundary conditions which made the near filed region results incorrect[11], [9]. The theory was then corrected using Babinet's principle which resulted in expression (8) for the electric field and expression (9) for the magnetic field, for wave propagation in z direction [9].

$$\bar{\mathbf{E}}(\mathbf{r}) = \begin{cases} \bar{E}_x = -\frac{4ik}{3\pi}\frac{2a^2-x^2-2y^2}{\sqrt{a^2-x^2-y^2}} \\ \bar{E}_y = -\frac{4ik}{3\pi}\frac{xy}{\sqrt{a^2-x^2-y^2}} \\ \bar{E}_z = 0 \end{cases} \tag{8}$$

$$\bar{\mathbf{H}}(\mathbf{r}) = \begin{cases} \bar{H}_x = 0 \\ \bar{H}_y = \frac{1}{\mu_0 c} \\ \bar{H}_z = -\frac{4}{\mu_0 c\pi}\frac{y}{\sqrt{a^2-x^2-y^2}} \end{cases} \tag{9}$$

Nevertheless, both Bethe and Bouwkamp reached the same conclusion, that hole structures can behave as an electric and magnetic dipole.

III. Light-matter Interactions

A. Surface Plasmons

As briefly mentioned before plasmons are a result of plasma oscillation and when this oscillation is given at a metal-dielectric interface, the plasmons are denominated Surface Plasmons (SPs).

The oscillation of the photons in light and the oscillation of plasma can couple and create a polariton, which appears due to the coupling of an EM wave (light) and an electric or magnetic dipole (nano-antenna). At a metal-dielectric interface, this phenomenon is called Surface Plasmon Polaritons (SPPs) and are essentially the metal's free electrons that oscillate in resonance with the incident light. This resonance phenomenon concentrates and amplifies the EM energy near the surface [9], [12].

In subwavelength structures, the SPPs concentrate light and enhance the electric field. However, two conditions must be met for polaritons to be created:

- At the incident light frequency, the metal must have an electric permittivity with a negative real part.
- The vector component of the incident light parallel to the interface should be matched with the wave number of the SPPs.

For optical frequencies, the first condition is met by metals, as gold, platinum and aluminium.

For subwavelength structures, like metal nanoparticles, the oscillation of the electron confined to the nano-structure creates Localized Surface Plasmons (LSPs) which, unlike SPs, do not propagate. This phenomenon creates a greatly enhanced electric field near the nano-particle.

B. Extraordinary Optical Transmission

The mentioned Bethe-Bowkamp diffraction theory assumed metal structures as perfect conductors. As such, for light incident in a slit, the smaller the aperture size, the lower the power transmitted. However, in 1998, Ebbessen et al. refuted this conclusion by discovering Extraordinary Optical Transmission (EOT).

The EOT phenomenon is verified when subwavelength structures transmit more light than predicted. Ebbesen conducted an experiment with an array of nano-sized cylindrical holes, with constant diameter and periodicity. The experiment showed transmission efficiency, normalized to the hole area, greater than the predicted by Bethe's theory, even reaching values above unity. This occurs due to the light coupling with SPs of the metal film and the creation of the polaritons that locally enhance the electric field and increase the transmission efficiency [13].

IV. Optical Properties

The optical properties of metals are a result of the conduction electrons moving freely in the material and the interband excitation when the photon's energy exceeds the metals' bandgap energy. The properties are described by a complex electric permittivity function dependent on the incident electromagnetic wave's frequency[14], [15].

$$\epsilon(\omega) = \epsilon_1(\omega) + i\epsilon_2(\omega) \tag{10}$$

The complex refractive index, in equation 11, is used to characterize the propagation of EM waves in a medium. The real part corresponds to the refractive index, n, which relates to the phase velocity and accounts for the dispersion losses, and the imaginary part corresponds to the extinction coefficient, k, which accounts for the attenuation of the EM waves and relates to the absorption coefficient and Ohmic losses. The complex permittivity and the complex refractive index relate to each other's real and imaginary parts through expressions 12 and 13.

$$N = n + ik \tag{11}$$

$$\epsilon_1 = n^2 - k^2 \tag{12}$$

$$\epsilon_2 = 2nk \tag{13}$$

The ohmic losses influence the field propagation near the surface and as such, affect the excitation of polaritons and their propagation. To mitigate these losses, one can either choose a material that possesses a dielectric function with a low module of its imaginary part or choose a material with a more negative real part of its dielectric function which will lower the refractive index and consequently decrease the penetration depth [15].

A. Drude-Lorentz model

In 1900, Paul Drude proposed a model to explain the transport properties of electrons in materials, namely metals [16]. Treating the conduction electrons in a metal as an ideal electron gas as a first approximation, the dielectric function of a metal can be expressed as in equation 14 where ω_p is the volume plasma frequency, and γ a damping constant [15].

$$\epsilon_{Drude}(\omega) = 1 - \frac{\omega_p^2}{\omega^2 + i\gamma\omega} \tag{14}$$

Initially, Drude used Maxwell-Boltzmann statistics but, in 1927, Sommerfeld replaced the statistics with Fermi-Dirac statistics which significantly improved the model.

Nevertheless, the Drude-Sommerfeld model does not account for interband transitions, as photons with enough energy can promote electrons from lower-lying valence bands to higher-energy conducting bands due to bound charges. In 1909, Hendrik Lorentz developed a model to describe the optical response of those charges. This additional degree of freedom is described by harmonic oscillators with defined resonance frequencies with contributions to the dielectric response of the type in equation 15 where $\tilde{\omega_p}$ depends on the density of bound electrons from the absorption process and $\tilde{\gamma}$ is a damping constant for the bound electrons [15].

$$\epsilon_{Lorentz}(\omega) = 1 + \frac{\tilde{\omega}_p^2}{(\omega_0^2 - \omega^2) - i\tilde{\gamma}\omega} \tag{15}$$

The Lorentz model employs oscillations in critical points corresponding to the interband transition energies which result in excessive absorption far from the critical points [1].

The Drude-Lorentz model is used to parameterize metal optical constants with expression (16) that contains two components. The first component corresponds to the Drude model and relates to the free-electron effects, and the second component corresponds to the Lorentz model and relates to the effects of the bound electrons and the interband transitions[1].

$$\hat{\epsilon}_r(\omega) = \hat{\epsilon}_r^{(f)}(\omega) + \hat{\epsilon}_r^{(b)}(\omega) \tag{16}$$

The contribution of bound electrons causes a deviation from the free electron gas model near ω_0 setting a maximum in the imaginary part of $\epsilon(\omega)$.

B. Fabry-Pérot-Like Resonance

When light waves are confined between two parallel reflecting surfaces a resonance can occur that is denominated Fabry-Pérot resonance. As the waves hit the surfaces they can be transmitted and reflected creating a standing wave pattern between surfaces. The created wave pattern has discrete resonant frequencies that depend on the distance between the surfaces and the refractive index of the medium between surfaces [17]. Additionally, in structures that confine light in a small region can occur multiple reflections of light which can cause resonances similar to the Fabry-Pérot[18] [19].

V. Simulations

Two aperture nanoantenna designs were simulated using COMSOL multiphysics software which makes use of the Finite Element Method (FEM) to solve complex physics problems. The simulated structure, of 1.2 um with and depth, was made of an air layer with 400 nm thickness followed by the aluminium nanoantenna layer, with an array of three by three apertures spaced 400 nm between them, on top of the amorphous silicon (a-Si) layer both with 50 nm thickness.

The simulations were conducted by doing a wavelength sweep between 400 nm and 2000 nm with a step of 5 nm which resulted in a total of 320 equidistant points. To measure field enhancement a probe was placed in the air within the apertures.

For the slot and the bowtie slot designs the following studies were conducted:

- Influence of the aperture size
- Influence of the gap size
- influence of the width size

Afterwards, the last two studies were repeated for a resized version of the two designs.

A. Slot Nanoantenna

The slot geometry was modelled after the one introduced in [20] with the same measurements and validated. Figure 1 shows an explicit representation of the slot shape and provides its base parameters. The software was capable of producing good results and thus it is possible to continue with the study.

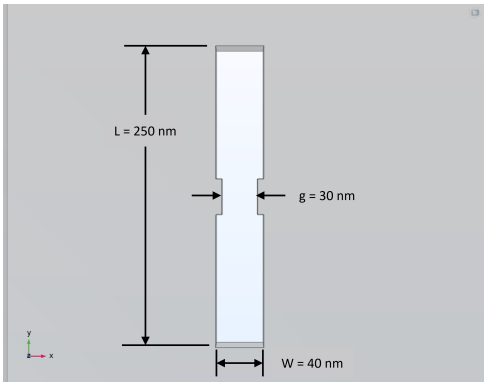

Fig. 1: Slot nanoantenna geometry and respective length L, width W, and gap g measurements.

1) Influence of the Slot Size: Firstly, the influence of the slot's size was studied. The slot dimensions were multiplied by a factor f in the x and y components and their results can be seen in figure 2. The measured EM field E is greater than the incident EM field E_0 which evidences the occurrence of the EOT phenomenon. There are visibly two main field enhancement regions, one located near 400 nm and another located near 1000 nm. Based on the findings of [19] where there are two resonance areas, the one in the shorter wavelengths was identified as the Fabry-Pérot-like resonance and the second region was identified as the plasmonic resonance.

Overall, as the slot size becomes smaller, the optical response magnitude increases and shifts to smaller wavelengths. From the original size to a resizing factor of 0.8 the magnitude of the optical response increases but the resonant wavelength remains the same. For the 0.6 and 0.4 resizing factors, the resonant peaks sharpen and reach a maximum magnitude of 22.06 for a wavelength of 995 nm for the smallest slot size. Table I shows the peak values and respective wavelengths for the resonance.

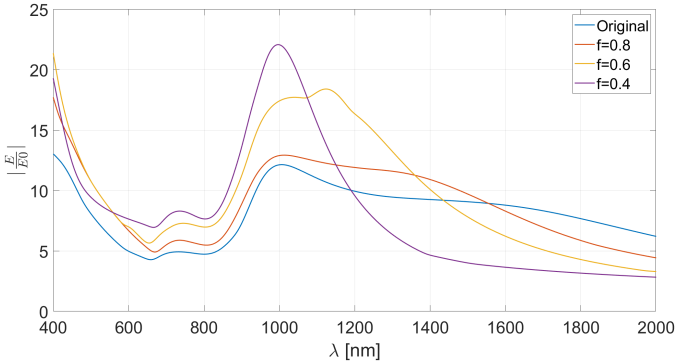

Fig. 2: Optical responses of the aluminium slot nanoantenna over a-Si with different resizing factors.

TABLE I: Resonance peak magnitude and wavelength values for the aluminium slot nanoantenna over a-Si with different resizing factors.

f	1	0.8	0.6	0.4
$\lvert\frac{E}{E_0}\rvert$	12.12	12.9	18.39	22.06
λ_{res} $[nm]$	1000	1000	1125	995

2) Influence of the Gap Size: Next, the influence of the gap size was studied. The results in figure 3 show that the measured EM field E is greater than the incident EM field E_0 and so, there is the occurrence of the EOT phenomenon. Similar to the previous results, there is also the formation of a higher field enhancement area near 400 nm, which, as seen before, is due to the Fabry-Pérot-like resonance.

Focusing on the plasmonic resonance there isn't always a shift to the longer wavelengths as the gap becomes smaller. The results show that when the gap is reduced from 30 nm to 20 nm the optical response shifts to the right, but when it is decreased from 20 nm to 15 nm and then to 10 nm, the optical response shifts to the left. However, the magnitude of the field enhancement progresses the same as the free-standing simulation where there is a decrease in magnitude as the gap size reduces from 30 nm to 20 nm, only to increase again as the gap decreases to 15 nm and 10 nm. The smallest gap size of 10 nm provides the results with the greatest field enhancement reaching a magnitude of 17.99 for a wavelength of 1060 nm. Table II shows the peak values and respective wavelengths for the resonance and figure 4 shows the relation between gap size and resonant wavelength.

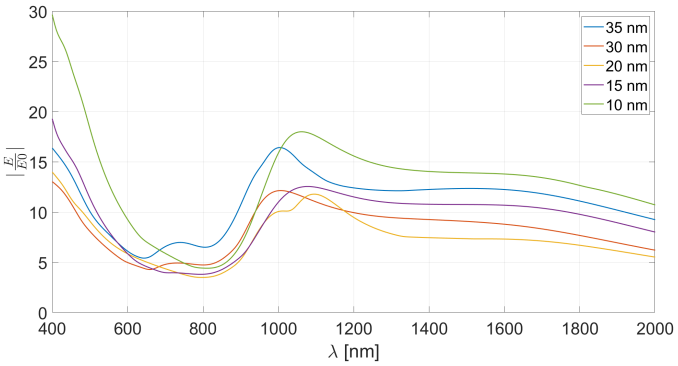

Fig. 3: Optical responses of the aluminium slot nanoantenna over a-Si with different gap sizes.

TABLE II: Resonance peak magnitude and wavelength values for the aluminium slot nanoantenna over a-Si with different gap sizes.

Gap [nm]	λ_{res} [nm]	$\lvert\frac{E}{E0}\rvert$
35	1005	16.42
30	1000	12.12
20	1090	11.78
15	1065	12.5
10	1060	17.99

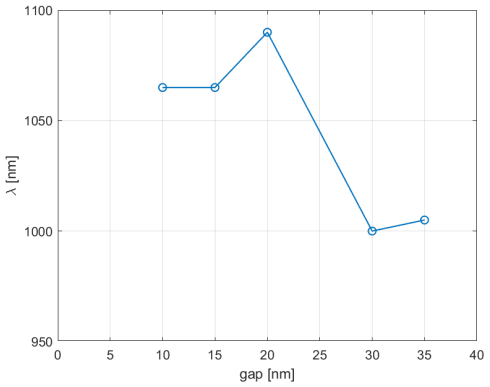

Fig. 4: Resonant wavelength variation with gap size of an aluminium slot nanoantenna over a-Si.

3) Influence of the Width Size: The influence of the width size on the optical response was studied. The simulation results in figure 5 show the occurrence of the EOT phenomenon since the measured EM field E is greater than the incident EM field E_0. Again, there are two significant field enhancement areas, being the first one denominated the Fabry-Pérot-like resonance and the second one the plasmonic resonance.

Focusing on the plasmonic resonance, as the slot width decreases, there is an increase in magnitude and a shift to the smaller wavelengths. The maximum field enhancement magnitude of 15.42 for a wavelength of 995 nm occurs at the 35 nm slot width. Table III shows the peak values and respective wavelengths for the resonance and figure 6 shows the non-linear relation between slot width and resonant wavelength.

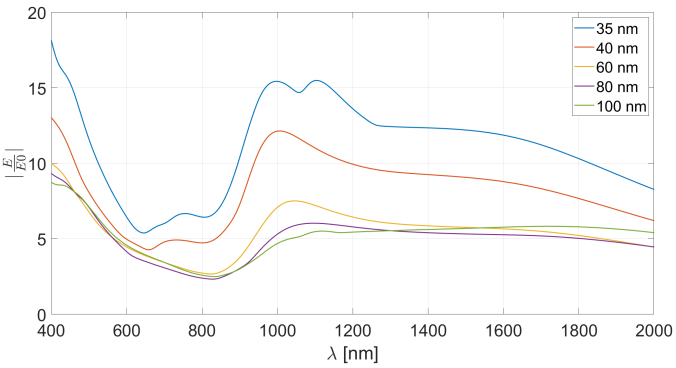

Fig. 5: Optical responses of the aluminium slot nanoantenna over a-Si with different width sizes.

The higher values of the magnitude of the optical response for the gap size variation results and for the width size variation results are similar in value. Only when the width size is higher does the magnitude reach lower values.

For both the gap size variation results and width size variation results, the plasmonic resonance occurs in the infrared spectrum and the Fabry-Pérot occurs in the visible spectrum.

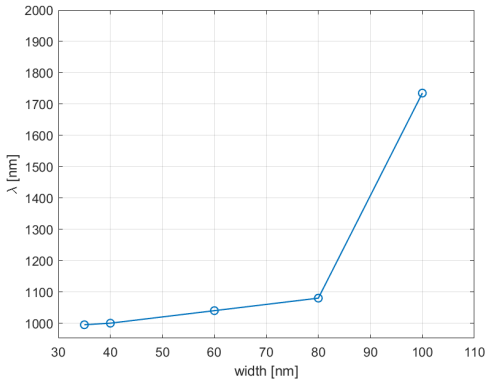

Fig. 6: Resonant wavelength variation with width size of an aluminium bowtie slot nanoantenna over a-Si.

TABLE III: Resonance peak magnitude and wavelength values for an aluminium slot nanoantenna over a-Si with different width sizes.

Width [nm]	λ_{res} [nm]	$\lvert\frac{E}{E0}\rvert$
100	1735	5.825
80	1080	6.016
60	1040	7.507
40	1000	12.12
35	995	15.42

B. Bowtie Slot Nanoantenna

The bowtie geometry was modelled after the slot bowtie from [19] with the same measurements and validated. Figure 7 shows an explicit representation of the slot shape and provides its base parameters.

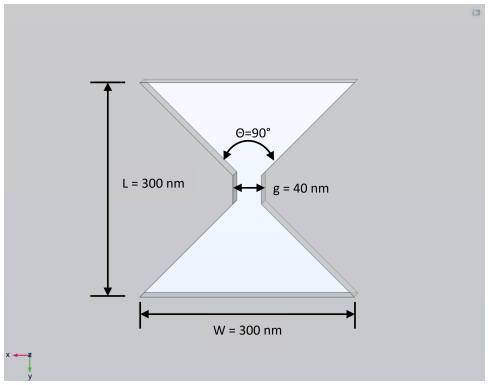

Fig. 7: Bowtie slot nanoantenna geometry and respective lengths a and b, flare angle θ, and gap g measurements.

1) Influence of the slot size: After the slot nanoantenna, the bowtie slot nanoantenna was simulated. The first simulation was done by resizing the slots with a factor f in the x and y direction. The obtained results can be seen in figure 8. The measured EM field E is greater than the incident EM E_0 field and so EOT phenomenon is present. Again, there is the formation of a higher field enhancement near 400 nm which can be due to the Fabry-Pérot-like resonance. Unlike previous results, there is only a clear plasmonic resonance peak for 1350 nm wavelength when the bowtie slot is resized with a factor of 0.4 and where it reaches a maximum magnitude of 8.176. For the resizing factor of 0.6, it is barely noticeable the onset of a maximum value near 1900 nm (evidenced by table IV) which continues to be at a magnitude much smaller than the previous simulations. Table 8 shows the peak values and respective wavelengths for the resonance.

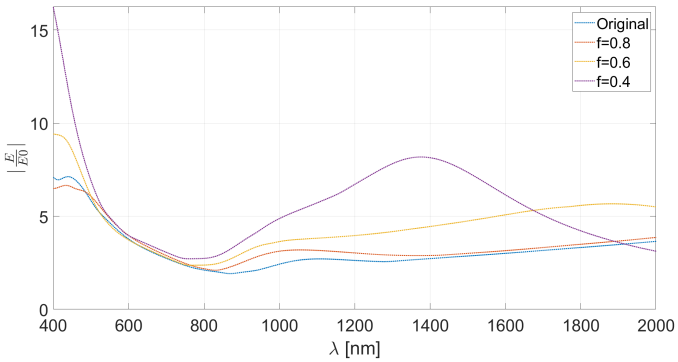

Fig. 8: Optical responses of the aluminium bowtie slot nanoantenna over a-Si with different resizing factors.

TABLE IV: Resonance peak magnitude and wavelength values for the aluminium bowtie slot nanoantenna over a-Si with different resizing factors.

f	1	0.8	0.6	0.4
$\lvert\frac{E}{E_0}\rvert$	-	-	5.66	8.176
λ_{res} $[nm]$	-	-	1900	1380

2) Influence of the gap size: To assess how the gap size influences the optical response, its value was varied and the results are presented in figure 9. The measured EM field E is greater than the incident EM field E_0 which proves the occurrence of the EOT phenomenon. The field enhancement near 400 nm mainly due to the Fabry-Pérot-like resonance is still present, however, there is no apparent plasmonic resonant behaviour.

Overall, the results vary little from one another as gap size varies, except for the 20 nm gap size where magnitude increases a bit more.

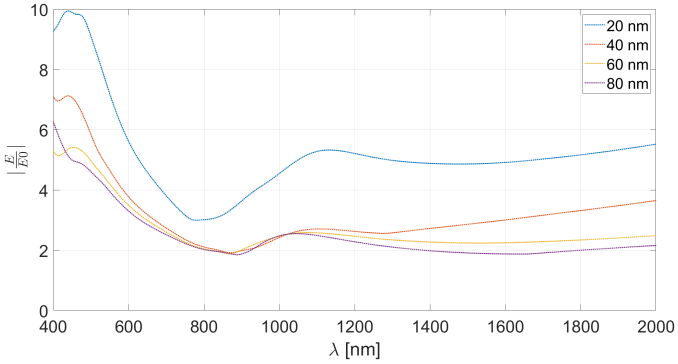

Fig. 9: Optical responses of the aluminium bowtie slot nanoantenna over a-Si with different gap sizes.

3) Influence of the width size: The influence of the width size can be seen in figure 10. There is the occurrence of the EOT phenomenon as the measured EM field E is greater than the incident EM field E_0. Similar to the previous simulation, there is a higher field enhancement region near 400 nm, but there is no apparent plasmonic resonance behaviour.

Overall, the results vary little from one another as the width size becomes smaller.

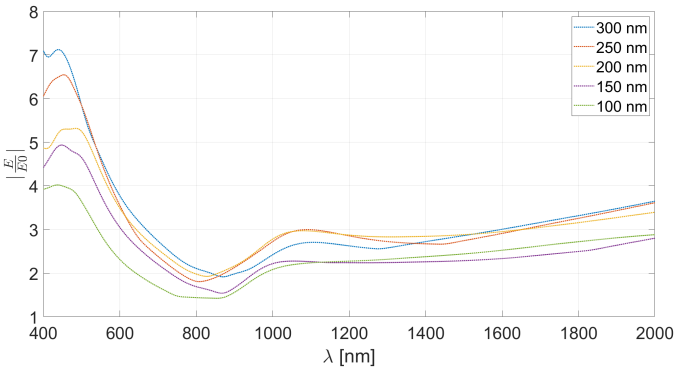

Fig. 10: Optical responses of the aluminium bowtie slot nanoantenna over a-Si with different width sizes.

Regarding the slot size variation for both geometries, the results show sharpness in the optical response as the slot becomes smaller with the smallest size reaching higher magnitude values and sharper resonance peaks.

The optical response of the slot nanoantenna changes similarly in magnitude by varying gap and width size. For the bowtie geometry, both the gap size and width size seem to have little influence on the optical response.

Overall, the slot nanoantenna reaches higher magnitude values than the bowtie slot nanoantenna.

RESIZED NANOANTENNAS

The original dimensions of the nanoantennas didn't perform very well on top of an a-Si layer. Looking at figures 2 and 8, it is clear that the nanoantennas with a resizing factor of 0.4 can produce a plasmonic resonant effect. With this in mind, the previous parameter variations were repeated but for a resizing factor of 0.4. To maintain the same variations, the resizing factor was applied after the parameter variation. For example, for a gap of 20 nm and a resizing factor of 0.4 the actual gap value is now 20*0.4=8 nm.

C. Resized Slot Nanoantenna

1) Influence of the gap size: The gap size for the resized slot nanoantenna was studied. The obtained results are shown in figure V and evidence the occurrence of the EOT phenomenon since the measured EM field E is greater than the incident EM field E_0. Again, there is an initial greater field enhancement near 400 nm that, as seen before, is mainly due to the Fabry-Pérot-like resonance caused by light confinement in small apertures. This initial enhancement is followed by a plasmonic resonance for longer wavelengths. There is an overall shift to smaller wavelengths as the gap becomes smaller. When the gap size is reduced from 35 nm up to 20 nm, the optical response magnitude decreases and when the size is reduced further to 15 nm and 10 nm the optical response increases again. The maximum magnitude of 37.47 for a wavelength of 1120 nm occurs when the gap is $10nm \times 0.4 = 4nm$. Table V shows the peak values and respective wavelengths for the plasmonic resonance and figure 12 shows the relation between gap size and resonant wavelength.

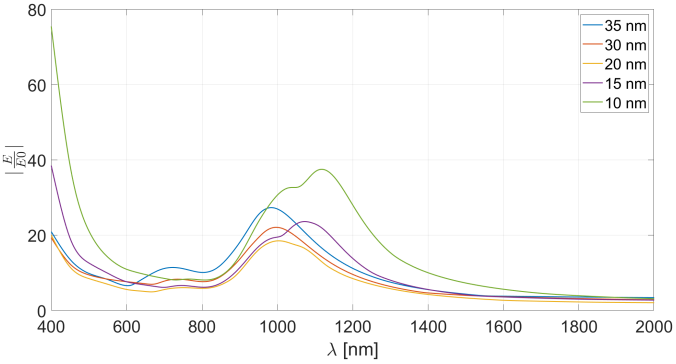

Fig. 11: Optical responses of the aluminium slot nanoantenna resized with a 0.4 factor over a-Si with different gap sizes.

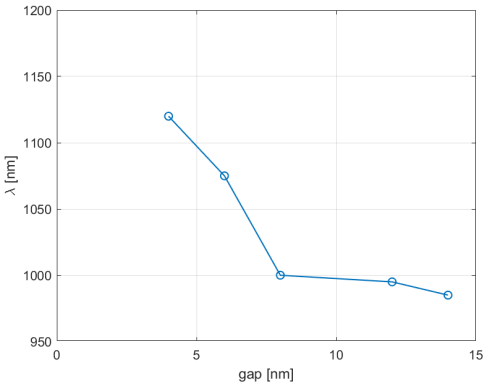

Fig. 12: Resonant wavelength variation with gap size of the resized aluminium slot nanoantenna over a-Si.

TABLE V: Resonance peak magnitude and wavelength values for the resized aluminium slot nanoantenna over a-Si with different gap sizes.

Gap [nm]	λ_{res} [nm]	$\lvert\frac{E}{E0}\rvert$
35×0.4	985	27.3
30×0.4	995	22.06
20×0.4	1000	18.47
15×0.4	1075	23.6
10×0.4	1120	37.47

2) Influence of the width size: The influence of the width size was studied for the resized slot nanoantenna and the results are presented in figure 13. Again, the measured EM field E is greater than the incident EM field E_0 thus proving the occurrence of the EOT phenomenon. There is an overall shift to higher wavelengths as the width size increases. Reducing the width size from 100 nm to 80 nm causes a decrease in

magnitude which increases again as the width is decreased further up to 35 nm. For the smallest two width sizes of 35 nm and 40 nm, the resonance occurs for the same wavelength of 995 nm. The greatest field enhancement magnitude of 29.61 for a wavelength of 995 nm occurs when the width size is $35nm \times 0.4 = 14nm$. Table VI shows the peak values and respective wavelengths for the plasmonic resonance and figure 14 shows the relation between gap size and resonant wavelength.

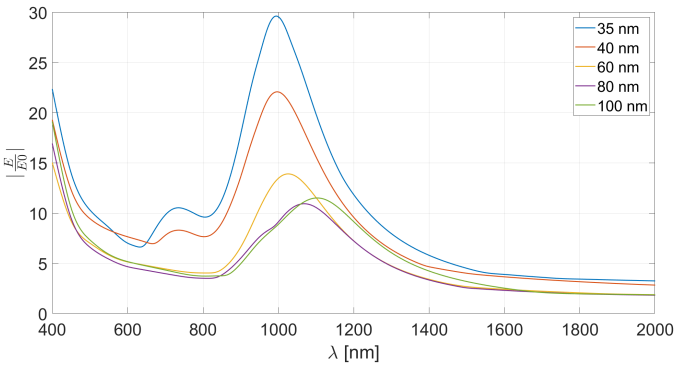

Fig. 13: Optical response of the aluminium slot nanoantenna resized with a 0.4 factor over a-Si with different width sizes.

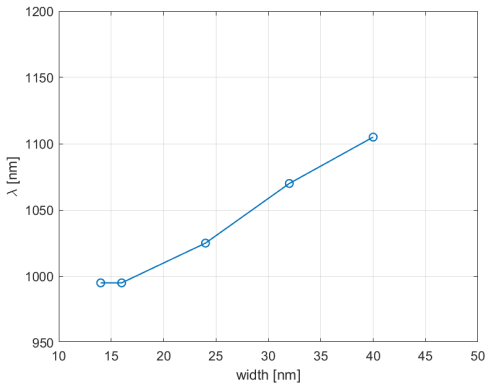

Fig. 14: Resonant wavelength variation with width size of the resized aluminium slot nanoantenna over a-Si.

TABLE VI: Resonance peak magnitude and wavelength values for the resized aluminium slot nanoantenna over a-Si with different width sizes.

Width [nm]	λ_{res} [nm]	$\lvert\frac{E}{E0}\rvert$
100×0.4	1105	11.5
80×0.4	1070	10.92
60×0.4	1025	13.89
40×0.4	995	22.06
35×0.4	995	29.61

The gap size variation and width size variation results have the plasmonic resonance occurring in the infrared spectrum. Reducing gap size caused the field enhancement near 400 nm to increase, but the width size variation did not have much effect on it. The gap size results produced peaks with a greater magnitude than the width variation results.

D. Resized Bowtie Slot Nanoantenna

1) Influence of the gap size: The influence of the gap size on the resized bowtie was studied and the results are seen in figure 15. The measured EM field E is greater than the incident EM field E_0 thus evidencing the occurrence of the EOT phenomenon. As in the previous simulations, there is an initial higher field enhancement near 400 nm, which, as seen before is caused by light confinement in small apertures. With gap size reduction, the optical response shifts to the longer wavelengths, its magnitude increases and the resonance peaks become sharper. The greatest field enhancement magnitude of 17.03 for a wavelength of 1410 nm occurs when the gap size is $20nm \times 0.4 = 8nm$. Table VII shows the peak values and respective wavelengths for the plasmonic resonance and figure 16 shows the relationship between gap size and resonant wavelength.

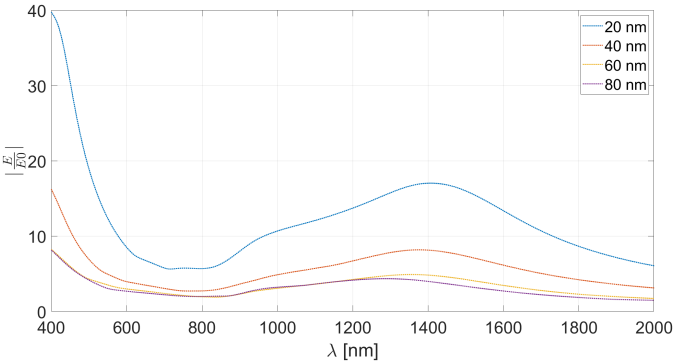

Fig. 15: Optical responses of the aluminium bowtie slot nanoantenna resized with a 0.4 factor over a-Si with different gap sizes.

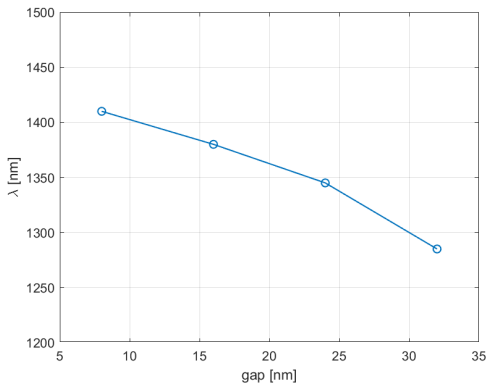

Fig. 16: Resonant wavelength variation with gap size of the resized aluminium bowtie slot nanoantenna over a-Si.

TABLE VII: Resonance peak magnitude and wavelength values for the resized aluminium bowtie slot nanoantenna over a-Si with different gap sizes.

Gap [nm]	λ_{res} [nm]	$\lvert\frac{E}{E0}\rvert$
80×0.4	1285	4.35
60×0.4	1345	4.86
40×0.4	1380	8.176
20×0.4	1410	17.03

2) Influence of the width size: The influence of width variation for the resized bowtie slot nanoantenna was studied and its results in figure 17 evidence the occurrence of the EOT phenomenon since the measured EM field E is greater than the incident EM field E_0. Again, near 400 nm there is a higher field enhancement due to the Fabry-Pérot-like resonance that occurs as light is confined in the small aperture. When the width size is reduced, there is an overall shift to the longer wavelengths and a decrease in magnitude. The greatest field enhancement magnitude of 8.176 for a wavelength of 1380 nm occurs when the gap size is $300nm \times 0.4 = 8nm$. Table VIII shows the peak values and respective wavelengths for the plasmonic resonance and figure 18 shows the relation between gap size and resonant wavelength.

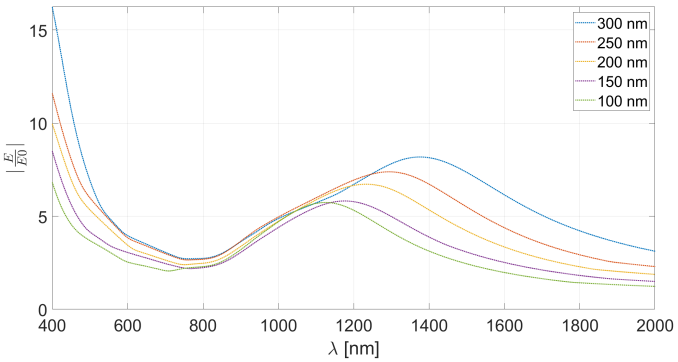

Fig. 17: Optical responses of the aluminium bowtie slot nanoantenna resized with a 0.4 factor over a-Si with different width sizes.

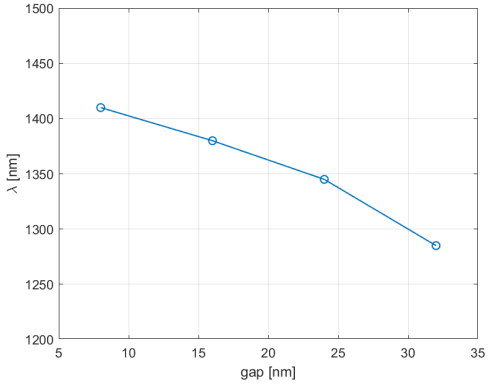

Fig. 18: Resonant wavelength variation with width size of the resized aluminium bowtie slot nanoantenna over a-Si.

TABLE VIII: Resonance peak magnitude and wavelength values for the resized aluminium bowtie slot nanoantenna over a-Si with different width sizes.

Width [nm]	λ_{res} [nm]	$\lvert\frac{E}{E0}\rvert$
300×0.4	1380	8.176
250×0.4	1295	7.38
200×0.4	1230	6.72
150×0.4	1180	5.82
100×0.4	1120	5.73

Both gap size and width size variation results have plasmonic resonance occurring in the infrared spectrum. The magnitude values of both responses do not vary much with the exception of the results for the smallest gap size which reaches higher values.

The resized slot produced optical responses higher in magnitude and with sharper plasmonic peaks than the resized bowtie slots.

VI. Conclusions

The objective of investigating the impact of coupling different nanoantennas in a a-Si layer was achieved. Understanding the individual influence of the different nanoantenna designs on the a-Si layer holds significant potential for defining diverse application areas. By leveraging the geometry of nanoantennas, one can aim for improved power conversion within various ranges of the light spectrum and complement the a-Si absorption capabilities.

The first important conclusion is that the measured EM field was always greater than the incident EM field which evidences that EOT phenomenon always occurs.

The analysis of the nanoantennas coupled to the a-Si layer showed that the slot geometry enables higher field enhancement magnitudes and sharper optical resonance curves.

For both geometries, high field enhancement and resonance occur in the infrared region. Additionally, the variation of the geometric parameters in both geometries had an impact on the optical response. Aperture size proved to be a very important parameter, as the optical response curves were significantly higher in magnitude and sharper for a smaller size than the original one. Overall, for the resized slot and bowtie slot nanoantennas, gap and width variation were able to influence both resonant wavelength and field enhancement magnitude. Particularly for the bowtie slot nanoantenna, the width size had the greatest influence on the resonant wavelength.

For all the simulations conducted with the nanoantennas coupled to the a-Si layer, an additional resonance was measured near 400 nm. As evidenced in the simulations, a secondary resonance in smaller wavelengths can occur due to the light confinement in the small aperture. This Fabry-Pérot-like resonance produced field enhancement magnitudes a lot larger than the plasmonic resonance.

Not only for light harvesting, and seeing how these structures have great performance in the infrared region, a possible application for the nanoantennas could be their usage in biosensors to help detect skin cancer.

Concluding, the objectives of this study were achieved as the optical response of the slot and bowtie slot geometries were obtained which allowed to conclude the impact the geometry of an aperture, and its respective geometric parameters, have on the optical response of an aperture nanoantenna and ultimately helped conclude on the capabilities of coupling nanoantennas to a a-Si absorber layer.

REFERENCES

[1] A. D. Rakić, A. B. Djurišić, J. M. Elazar, and M. L. Majewski, "Optical properties of metallic films for vertical-cavity optoelectronic devices," *Appl. Opt.*, vol. 37, no. 22, pp. 5271–5283, Aug 1998. [Online]. Available: http://opg.optica.org/ao/abstract.cfm?URI=ao-37-22-5271

[2] C. Reynaud, D. Duché, J.-J. Simon, E. Sanchez-Adaime, O. Margeat, J. Ackermann, V. Jangid, C. Lebouin, D. Brunel, F. Dumur, D. Gigmes, G. Berginc, C. Nijhuis, and L. Escoubas, "Rectifying antennas for energy harvesting from the microwaves to visible light: A review," *Progress in Quantum Electronics*, vol. 72, p. 100265, 2020. [Online]. Available: https://www.sciencedirect.com/science/article/pii/S0079672720300197

[3] M. S.A, *Plasmonics: Fundamentals and Applications*. Springer, 2007.

[4] A. E. Krasnok, I. S. Maksymov, A. I. Denisyuk, P. A. Belov, A. E. Miroshnichenko, C. R. Simovski, and Y. S. Kivshar, "Optical nanoantennas," *Physics-Uspekhi*, vol. 56, no. 6, pp. 539–564, jun 2013. [Online]. Available: https://doi.org/10.3367/ufne.0183.201306a.0561

[5] Q.-H. Park, "Optical antennas and plasmonics," *Contemporary Physics*, vol. 50, no. 2, pp. 407–423, 2009. [Online]. Available: https://doi.org/10.1080/00107510902745611

[6] J. Wenger, "Aperture optical antennas," 05 2014.

[7] B. D. Guenther, *Modern Optics*. Oxford University Press, 10 2015. [Online]. Available: https://doi.org/10.1093/acprof:oso/9780198738770.001.0001

[8] B. Kapralos, M. Jenkin, and E. Milios, "Acoustical diffraction modeling utilizing the huygens-fresnel principle," in *IEEE International Workshop on Haptic Audio Visual Environments and their Applications*, 2005, pp. 6 pp.–.

[9] R. A. Marques Lameirinhas, J. P. N. Torres, and A. Baptista, "A sensor based on nanoantennas," *Applied Sciences*, vol. 10, no. 19, 2020. [Online]. Available: https://www.mdpi.com/2076-3417/10/19/6837

[10] R. Fitzpatrick. Young's double-slit experiment. (2022, August 23). [Online]. Available: https://farside.ph.utexas.edu/teaching/316/lectures/node151.html

[11] R. D. F. Gomes, M. Martins, A. Baptista, and J. P. Torres, "Study of a nano optical antenna for intersatellite communications," *Optical and Quantum Electronics*, vol. 49, 03 2017.

[12] I. Caetano, J. P. Torres, and R. Lameirinhas, "Simulation of solar cells with integration of optical nanoantennas," *Nanomaterials*, 01 2021.

[13] H. Mekawey, M. Swillam, and Y. Ismail, "Extraordinary optical transmission in silicon nanoholes," *Scientific Reports*, vol. 11, 11 2021.

[14] L. Novotny and B. Hecht, *Principles of Nano-Optics*. Cambridge University Press, 2006.

[15] P. Biagioni, J.-S. Huang, and B. Hecht, "Nanoantennas for visible and infrared radiation," *Reports on progress in physics. Physical Society (Great Britain)*, vol. 75, p. 024402, 02 2012.

[16] P. Drude, "Zur elektronentheorie der metalle," *Annalen der Physik*, vol. 306, no. 3, pp. 566–613, 1900. [Online]. Available: https://onlinelibrary.wiley.com/doi/abs/10.1002/andp.19003060312

[17] E. Hecht, *Optics*. Pearson Education, 2002.

[18] J. D. Joannopoulos, S. G. Johnson, J. N. Winn, and R. D. Meade, *Photonic Crystals: Molding the Flow of Light*. Princeton University Press, 2011.

[19] H. Guo, T. P. Meyrath, T. Zentgraf, N. Liu, L. Fu, H. Schweizer, and H. Giessen, "Optical resonances of bowtie slot antennas and their geometry and material dependence," *Opt. Express*, vol. 16, no. 11, pp. 7756–7766, May 2008. [Online]. Available: https://opg.optica.org/oe/abstract.cfm?URI=oe-16-11-7756

[20] V. Dinesh kumar and K. Asakawa, "Investigation of a slot nanoantenna in optical frequency range," *Photonics and Nanostructures - Fundamentals and Applications*, vol. 7, no. 3, pp. 161–168, 2009. [Online]. Available: https://www.sciencedirect.com/science/article/pii/S1569441009000340